ENERGY SPECTRA, E2 TRANSITION PROBABILITIES AND SHAPE DEFORMATIONS FOR THE EVEN-EVEN ISOTOPES $^{180-196}$Pt

P. BUGANU[1], A.A. RADUTA[1,2]

[1]Department of Theoretical Physics,
"Horia Hulubei" National R&D Institute for Physics and Nuclear Engineering,
Reactorului 30, RO-077125, POB-MG6, Măgurele-Bucharest, Romania, EU
E-mail: buganu@theory.nipne.ro
[2]Academy of Romanian Scientists,
54 Splaiul Independentei, Bucharest 050094, Romania

Received May 28, 2014

The even-even isotopes of the $^{180-196}$Pt chain are analyzed in the framework of two solvable approaches for the quadrupole intrinsic variables, called the Davidson and Spheroidal Approach (DSA) and Davidson and Mathieu Approach (DMA), respectively. The energy spectra of the ground and first β and γ bands, E2 transition probabilities between states belonging to these bands and shapes of the ground and some excited states are determined for each isotope. The numerical results are compared with the corresponding experimental data as well as with those obtained with two recently proposed models, namely, the Sextic and Spheroidal Approach (SSA) and Sextic and Mathieu Approach (SMA).

Key words: Isotopes of Platinum, collective models, energy spectra, E2 transitions, nuclear shapes.

PACS: 21.60.Ev, 21.10.Re, 27.70.+q, 27.80.+w.

1. INTRODUCTION

Recently [1], the present authors have applied several solvable approaches as the Sextic and Spheroidal Approach (SSA) [2], the Sextic and Mathieu Approach (SMA) [3], the Infinite Square Well and Spheroidal Approach (ISWSA) [4] and the Infinite Square Well and Mathieu Approach (ISWMA) [1], respectively, to describe the properties of the even-even isotopes of the $^{180-196}$Pt chain. Numerical results for energy spectra and E2 transition probabilities were compared with the corresponding experimental data as well as with those yielded by the X(5) [5] and Z(5) [6] approaches. This comparison revealed that the SSA and SMA offer a better description of the experimental data than the other approaches. Additionally, the contour plots of the probability density as a function of the intrinsic dynamic variables pointed out a shape evolution along the isotope chain.

Properties of the isotopes of Platinum as energy spectra, B(Eλ) transition probabilities, shape coexistence and shape evolution were largely analyzed and discussed from both theoretical and experimental point of view in many papers [6–19].

In the present work, other two approaches will be applied for the isotope chain $^{180-196}$Pt, namely, the Davidson and Spheroidal Approach (DSA) [20] and Davidson and Mathieu Approach (DMA), respectively, hopping to bring new contributions in explaining the experimental data. While the DSA was earlier proposed in Ref. [2], the DMA is an unedited approach described in Sec. II. Numerical results obtained with the DSA and DMA are compared with the experimental data of the isotope chain $^{180-196}$Pt as well as with those yielded by the SSA and SMA in Sec. III, in order to see how these approaches complement each other. In addition, using the wave functions of the DSA and DMA, the contour plots of the probability density are represented in polar coordinates for the ground state and some excited states for each even-even isotope of the chain. Finally, the main conclusions are collected in Sec. IV.

2. DESCRIPTION OF THE DAVIDSON AND MATHIEU APPROACH

2.1. THE MODEL HAMILTONIAN AND SEPARATION OF VARIABLES

Due to the fact that the SSA, SMA and DSA were proposed and largely discussed in previous papers [1–3, 20–23], they will not be presented here. Instead, the Davidson and Mathieu Approach will be described in detail. The starting point is the Bohr-Mottelson Hamiltonian [24],

$$H=-\frac{\hbar^2}{2B}\left[\frac{1}{\beta^4}\frac{\partial}{\partial\beta}\beta^4\frac{\partial}{\partial\beta}+\frac{1}{\beta^2\sin 3\gamma}\frac{\partial}{\partial\gamma}\sin 3\gamma\frac{\partial}{\partial\gamma}-\frac{1}{4\beta^2}\sum_{k=1}^{3}\frac{\hat{Q}_k^2}{\sin^2(\gamma-\frac{2\pi}{3}k)}\right]+ \\ +C\frac{\beta^2}{2}, \quad (1)$$

amended with a potential [26, 27]

$$V(\beta,\gamma)=V_1(\beta)+\frac{V_2(\gamma)}{\beta^2}, \quad (2)$$

which allows us to separate the β deformation variable from the other four, the axial deformation variable γ and the three Euler angles θ_1, θ_2 and θ_3, which remain coupled due to the rotor term. $\hat{Q}_k$ denote the angular momentum components in the intrinsic reference frame. A full separation of variables is achieved [3] by expanding the rotor term, denoted hereafter with W, in power series of γ, around $\gamma_0=30^0$,

$$W\approx(Q^2-\frac{3}{4}Q_1^2)+2\sqrt{3}(Q_2^2-Q_3^2)\left(\gamma-\frac{\pi}{6}\right)+(10Q^2-\frac{39}{4}Q_1^2)\left(\gamma-\frac{\pi}{6}\right)^2, \quad (3)$$

and then averaging the result with the Wigner function $W^L_{MR}(\theta_1,\theta_2,\theta_3)$,

$$\langle W\rangle\approx L(L+1)-\frac{3}{4}R^2+\left(10L(L+1)-\frac{39}{4}R^2\right)\left(\gamma-\frac{\pi}{6}\right)^2. \quad (4)$$

In Eq. (4), $L(L+1)$ and R are the eigenvalues of the operators $\hat{Q}^2$ and $\hat{Q}_1$, respectively. The first term $L(L+1)$ and the rest terms of Eq. (4), multiplied by $1/\beta^2$, are added to the β and γ equations, respectively:

$$\left[-\frac{1}{\beta^4}\frac{d}{d\beta}\beta^4\frac{d}{d\beta}+\frac{L(L+1)}{\beta^2}+v_1(\beta)\right]f(\beta)=\varepsilon_\beta f(\beta), \tag{5}$$

$$\left[-\frac{1}{\sin 3\gamma}\frac{d}{d\gamma}\sin 3\gamma\frac{d}{d\gamma}-\frac{3}{4}R^2+\left(10L(L+1)-\frac{39}{4}R^2\right)\left(\gamma-\frac{\pi}{6}\right)^2+v_2(\gamma)\right]\phi(\gamma)= \\ =\tilde{\varepsilon}_\gamma\phi(\gamma). \tag{6}$$

In Eqs. (5,6) the following notations are introduced:

$$v_1(\beta)=\frac{2B}{\hbar^2}V_1(\beta),\quad v_2(\gamma)=\frac{2B}{\hbar^2}V_2(\gamma),\quad \varepsilon_\beta=\frac{2B}{\hbar^2}E_\beta,\quad \tilde{\varepsilon}_\gamma=\langle\beta^2\rangle\frac{2B}{\hbar^2}E_\gamma. \tag{7}$$

Here, with $\langle\beta^2\rangle$ is denoted the average value of β^2 which further it will be treated as a free parameter. In Ref. [2] it is shown that this is a reasonable approximation. For some conditions, concerning the separation of variables, the problem can be exactly solved [25]. The solutions of the resulting equations (5,6) depend on the potential forms. In what follows, these equations will be discussed separately.

2.2. SOLUTION OF THE β EQUATION

Considering a Davidson type potential [28] for the β variable,

$$v_1(\beta)=a_1\beta^2+\frac{a_2^4}{\beta^2}, \tag{8}$$

and making the change of function $f(\beta)=\beta^{-2}\psi(\beta)$, Eq. (5) is reduced to the form:

$$\left[\frac{d^2}{d\beta^2}+\varepsilon_\beta-\frac{L(L+1)+a_2^4+2}{\beta^2}-a_1\beta^2\right]\psi(\beta)=0. \tag{9}$$

The potential given by Eq. (8) has a minimum at $\beta_0=a_1^{-1/4}a_2$ which is equal with a_2 when $a_1=1$. In numerical calculations a_1 will be treated as a free parameter in order the potential (8) to have a minimum at β_0 close to the experimental nuclear deformation. After a suitable change of function and variable in Eq. (9), the final solution is expressed in terms of the generalized Laguerre polynomials $L_{n_\beta}^{m_\beta}$,

$$\begin{aligned} f_{n_\beta,m_\beta}(\beta)&=\sqrt{\frac{2(\sqrt{a_1})^{m_\beta+1}n_\beta!}{\Gamma(n_\beta+m_\beta+1)}}L_{n_\beta}^{m_\beta}(\sqrt{a_1}\beta^2)\beta^{m_\beta-\frac{3}{2}}e^{-\frac{\sqrt{a_1}\beta^2}{2}},\\ m_\beta&=\sqrt{L(L+1)+\frac{9}{4}+a_2^4}, \end{aligned} \tag{10}$$

where Γ is the Euler gamma function. The corresponding eigenvalues are given by:

$$E_\beta(n_\beta,L)=\frac{\hbar^2}{2B}2\sqrt{a_1}\left(2n_\beta+1+\sqrt{L(L+1)+\frac{9}{4}+a_2^4}\right),\ \ n_\beta=0,1,2,\dots\ . \quad (11)$$

The solution of the β equation with a Davidson potential was used before in Refs. [6, 20, 29–34]. The new thing here is the use, at a time, of the solution in β just mentioned and the Mathieu solution for the γ equation, which results in obtaining of a solvable approach for the generalized Bohr-Mottelson Hamiltonian (1,2), conventionally called the Davidson and Mathieu Approach (DMA).

2.3. SOLUTION OF THE γ EQUATION

The Mathieu solution for the γ variable was proposed in Ref. [4] for axial symmetric deformed nuclei and then in Ref. [3] to describe triaxial nuclei having γ_0 close 30^0. Hereinafter, the second procedure will be applied. Therefore, a periodic potential is considered for Eq. (6),

$$v_2(\gamma)=u_2\cos^2 3\gamma,\quad u_2>0, \quad (12)$$

which has a minimum at $\gamma_0=30^0$. Further, with the change of function $\phi(\gamma)=\eta(\gamma)/\sqrt{|\sin 3\gamma|}$, Eq. (6) becomes

$$\begin{aligned}&\left[\frac{d^2}{d\gamma^2}+\frac{9}{4\sin^2 3\gamma}+\left(\tilde{\varepsilon}_\gamma+\frac{9}{4}+\frac{3}{4}R^2\right)\right]\eta(\gamma)-\\&-\left[\left(10L(L+1)-\frac{39}{4}R^2\right)\left(\gamma-\frac{\pi}{6}\right)^2+v_2(\gamma)\right]\eta(\gamma)=0.\end{aligned} \quad (13)$$

To obtain the Mathieu equation, other two steps are performed, namely, the approximations

$$\frac{9}{4\sin^2 3\gamma}\approx\frac{9}{4}+\frac{81}{4}\left(\gamma-\frac{\pi}{6}\right)^2,\ \ \left(\gamma-\frac{\pi}{6}\right)^2\approx\frac{1}{9}\cos^2 3\gamma, \quad (14)$$

and the change of variable $y=3\gamma$, respectively:

$$\left(\frac{d^2}{\partial y^2}+a_{n_\gamma}-2q\cos 2y\right)\mathcal{M}(y)=0, \quad (15)$$

$$q=\frac{1}{36}\left(\frac{10}{9}L(L+1)-\frac{13}{12}R^2+u_2-\frac{9}{4}\right),\ \ a_{n_\gamma}=\frac{1}{9}\left(\tilde{\varepsilon}_\gamma+\frac{3}{4}R^2+\frac{9}{2}\right)-2q. \quad (16)$$

In Eq. (15), $\mathcal{M}(y)$ is the Mathieu function satisfying the orthonormalization condition:

$$\frac{6}{\pi}\int_0^{\frac{\pi}{3}}\mathcal{M}_n(y)\mathcal{M}_m(y)dy=\delta_{nm}. \quad (17)$$

The corresponding energy is easily found from Eq. (16) by using the expression of the characteristic value a_{n_γ}:

$$E_\gamma(n_\gamma, L, R) = \frac{\hbar^2}{2B}\frac{1}{\langle\beta^2\rangle}\left[9a_{n_\gamma}(L,R) + 18q(L,R) - \frac{3}{4}R^2 - \frac{9}{2}\right], \quad n_\gamma = 0, 1, 2, \ldots \quad (18)$$

The total energy corresponding to the DMA is given by the sum of the β and γ equation eigenvalues:

$$\begin{aligned} E(n_\beta, n_\gamma, L, R) =& G\left[2\sqrt{a_1}\left(2n_\beta + 1 + \sqrt{L(L+1) + \frac{9}{4} + a_2^4}\right)\right] + \\ &+ F\left[9a_{n_\gamma}(L,R) + 18q(L,R) - \frac{3}{4}R^2 - \frac{9}{2}\right], \end{aligned} \quad (19)$$

where $G = \frac{\hbar^2}{2B}$ and $F = \frac{1}{\langle\beta^2\rangle}\frac{\hbar^2}{2B}$. The values for the quantum numbers n_β, n_γ, L, R corresponding to the ground and first β and γ bands are the following:

$$\begin{aligned} &n_\beta = 0,\ n_\gamma = 0, \quad R = L, \qquad L = 0, 2, 4, \ldots \quad \text{ground band,} \\ &n_\beta = 0,\ n_\gamma = 1, \begin{cases} R = L-2, L = 2, 4, 6, ... \\ R = L-1, L = 3, 5, 7, ... \end{cases} \text{gamma band,} \\ &n_\beta = 1,\ n_\gamma = 0, \quad R = L, \qquad L = 0, 2, 4, \ldots \quad \text{beta band.} \end{aligned} \quad (20)$$

The total wave function of the system is:

$$\begin{aligned} |LRMn_\beta n_\gamma\rangle =& N_{L,n_\beta} f_{L,n_\beta}(\beta)\sqrt{\frac{6}{\pi}}\mathcal{M}_{L,R,n_\gamma}(3\gamma)\cdot \\ &\cdot\sqrt{\frac{2L+1}{16\pi^2(1+\delta_{R0})}}\left(D^L_{MR}(\Omega) + (-1)^L D^L_{M-R}(\Omega)\right), \end{aligned} \quad (21)$$

where N_{L,n_β} are the normalization constants of the β functions.

2.4. ELECTROMAGNETIC TRANSITIONS

The reduce $E2$ transition probabilities,

$$B(E2, i \to f) = |\langle L_i R_i M_i n_{\beta i} n_{\gamma i} || T_2^{(E2)} || L_f R_f M_f n_{\beta f} n_{\gamma f}\rangle|^2, \quad (22)$$

written in the Rose's convention [35] are determined by taking in consideration also the anharmonic contribution of the quadrupole transition operator:

$$T^{(E2)}_{2\mu} = t_1\beta\left[\cos\left(\gamma-\frac{2\pi}{3}\right)D^2_{\mu 0}+\frac{1}{\sqrt{2}}\sin\left(\gamma-\frac{2\pi}{3}\right)(D^2_{\mu 2}+D^2_{\mu,-2})\right]+$$
$$+t_2\sqrt{\frac{2}{7}}\beta^2\left[-\cos\left(2\gamma-\frac{4\pi}{3}\right)D^2_{\mu 0}+\frac{1}{\sqrt{2}}\sin\left(2\gamma-\frac{4\pi}{3}\right)(D^2_{\mu 2}+D^2_{\mu,-2})\right].$$

Using the argument $\gamma-2\pi/3$ instead of γ, in Eq. (23), is justified by the fact that here R, the eigenvalue of the operator Q_1, is a good quantum number and not K which corresponds to Q_3. This replacement was also used in Ref. [6], where the Z(5) approach was proposed.

3. NUMERICAL RESULTS

The Davidson and Mathieu Approach (DMA), introduced here, together with the DSA will be applied for the description of the isotope chain $^{180-196}$Pt. The applications will be made by taking into account the signatures defined below:

$$R_{4_g^+/2_g^+}=\frac{E_{4_g^+}-E_{0_g^+}}{E_{2_g^+}-E_{0_g^+}},\quad R_{0_\beta^+/2_g^+}=\frac{E_{0_\beta^+}-E_{0_g^+}}{E_{2_g^+}-E_{0_g^+}},\tag{23}$$

whose values are given for each isotope in Table 1 .

Table 1

The ratios $R_{4_g^+/2_g^+}$ and $R_{0_\beta^+/2_g^+}$, given by Eq. (23), corresponding to each isotope of the chain $^{180-196}$Pt are compared with those of X(5), Z(5) and O(6).

	^{180}Pt	^{182}Pt	^{184}Pt	^{186}Pt	^{188}Pt	^{190}Pt	^{192}Pt	^{194}Pt	^{196}Pt	X(5)	Z(5)	O(6)
$R_{4_g^+/2_g^+}$	2.69	2.71	2.67	2.55	2.52	2.49	2.48	2.47	2.46	2.90	2.35	2.50
$R_{0_\beta^+/2_g^+}$	3.12	3.23	3.02	2.46	3.00	3.11	3.78	3.86	3.19	5.65	3.91	-

According to the ratio $R_{4_g^+/2_g^+}$, the isotopes ^{180,182,184}Pt are close to X(5) picture, while the rest ^{186,188,190,192,194,196}Pt would belong to the O(6) dynamical symmetry. For ^{186}Pt, because $E_{2_\gamma^+}>E_{0_\beta^+}$, we can say that this isotope has a stable γ deformation rather than a $\gamma-$unstable one. Instead, the ratio $R_{0_\beta^+/2_g^+}$ recommend the isotopes ^{192,194}Pt as good candidates for Z(5), but not for for X(5). From these observations we may conclude that this isotope chain manifests partial properties for critical points of the shape phase transitions U(5)→SU(3) and SU(3)→$\overline{\mathrm{SU(3)}}$, respectively. In conclusion, it is difficult to say exactly which is the most appropriate description for each isotope. What is interesting instead is that in Ref. [1], the SSA

and SMA applications for $^{180-188}$Pt and $^{190-196}$Pt, respectively, were able to explain some additional properties of these nuclei which couldn't be reproduced in the framework of X(5) and Z(5). For example, the SSA eliminated the drawback of X(5) in explaining the head state of the β band for ^{180,182,184}Pt, especially for the isotope ^{182}Pt which, as suggested in Ref. [14], has some X(5) features. Another example is that of the SMA which provided a good description for the γ band of $^{190-196}$Pt, especially for the staggering behavior of ^{192}Pt where Z(5) results are far from the experimental data. Following the same path as in Ref. [1], the DSA and DMA will be applied for the isotopes $^{180-188}$Pt and $^{190-196}$Pt, respectively, and the results will be compared also with those yielded by the SSA and SMA in order to see what are the new contributions in explaining the corresponding experimental data.

The parameters of the DSA, DMA, SSA and SMA, fixed by fitting some experimental data, are given in Tables 2,3.

Table 2

Parameters of the DSA and SSA fitted for the experimental data of $^{180-188}$Pt.

	G [keV]		F [keV]		u_1		u_2		a_1	a_2	a	b	$t_1[W.u.]^{\frac{1}{2}}$		$t_2[W.u.]^{\frac{1}{2}}$	
Nucl	DSA	SSA	DSA	SSA	DSA	SSA	DSA	SSA	DSA	DSA	SSA	SSA	DSA	SSA	DSA	SSA
^{180}Pt	2.718	1.04	37.91	3.34	-975.5	-821.2	474.2	-1000	4528	1.873	1059	135	1392	1750	0	0
^{182}Pt	2.512	0.812	29.07	5.326	-16.71	-1042	-23.35	-0.001	5344	1.581	1687	186	4215	6561	33465	89567
^{184}Pt	2.555	0.624	28.47	6.248	-99.31	-302.6	12.99	-262	4863	1.582	3030	256	4005	7821	30255	122065
^{186}Pt	1.917	0.846	39.95	3.085	-430.8	1471	219.9	-2326	5635	1.088	1296	170	3792	5061	25902	58515
^{188}Pt	4.957	1.453	34.75	14.55	-500	-466.2	293.1	165.8	1766	0.818	1449	95	1259	1717	0	0

Table 3

Parameters of the DMA and SMA fitted for the experimental data of $^{190-196}$Pt.

	G [keV]		F [keV]		u_2		a_1	a_2	a	b	$t_1[W.u.]^{\frac{1}{2}}$		$t_2[W.u.]^{\frac{1}{2}}$	
Nucl	DMA	SMA	DMA	SMA	DMA	SMA	DMA	DMA	SMA	SMA	DMA	SMA	DMA	SMA
^{190}Pt	2.184	1.114	6.287	8.143	133.4	104.6	11040	2.204	3014	84	70.43	96.38	0	0
^{192}Pt	3.581	2.952	7.577	7.867	107.7	121.8	6627	2.583	616.5	22.98	51.11	55.1	878.2	1048
^{194}Pt	3.236	2.957	12.06	14.68	43.04	32.74	9351	2.477	733	33.05	39.48	43.43	1082	1077
^{196}Pt	2.210	0.411	5.148	6.455	221.9	177	14705	2.272	28322	250	54.35	130.2	2071	11224

As seen in Fig.1, they have a smooth dependence on the atomic mass A. Indeed the values corresponding to the considered isotopes were interpolated by simple polynomial functions. We notice that a_1, a_2 and u_1 have minima either in $A = 186$ or for A=188. By contrast the parameters G, F and u_2 have maxima in the mentioned points. The change of sign of the first derivatives for these nuclei might be tentatively interpreted as a critical point for a phase transition.

The numerical results for the energy spectra are compared with the experimental data in Figs. 2,3,4. By analyzing the ground band description given by the DSA

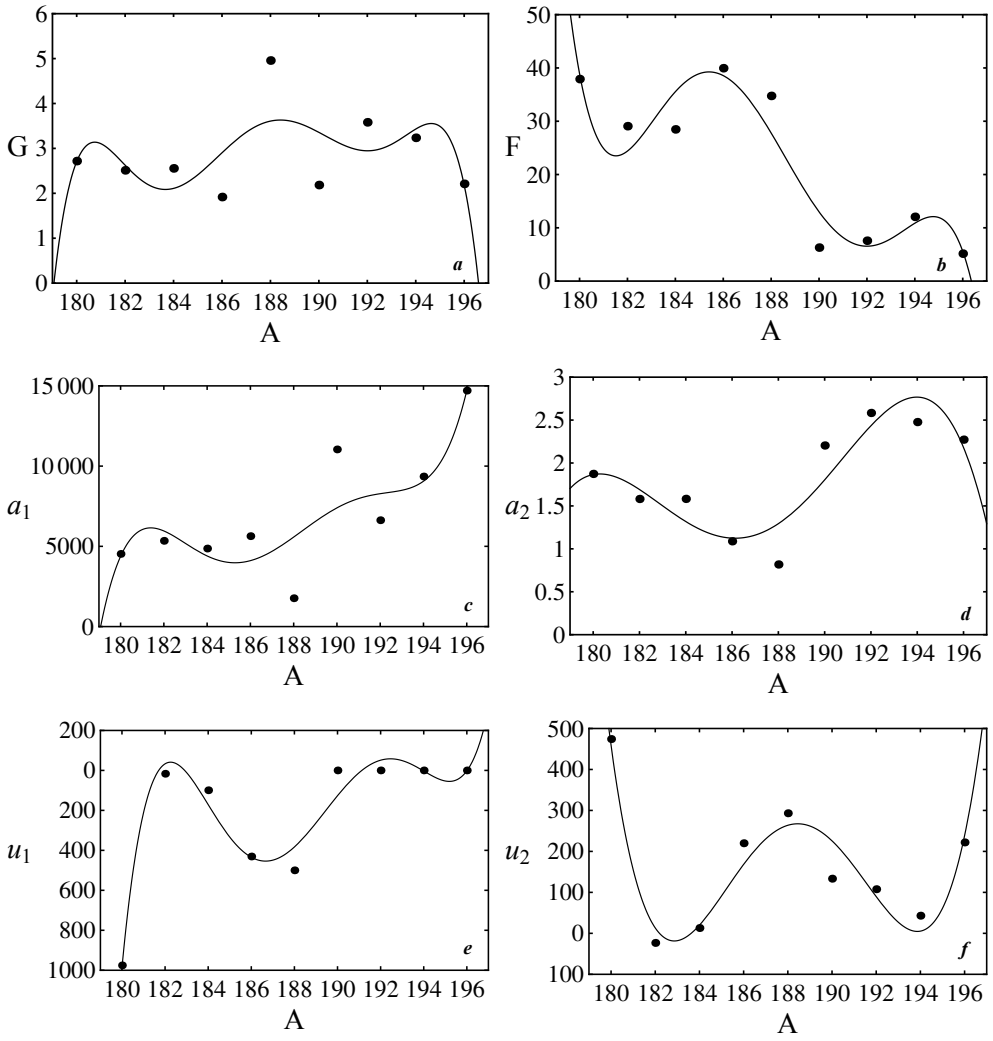

Fig. 1 – The parameters G, F, a_1, a_2, u_1 and u_2 are represented as function of A.

and SSA for the isotopes $^{180-188}$Pt we can observe that both approaches are close to the experimental data and that happens even for high spin states. For the β band, the DSA has problems in reproducing the energy of the 0^+ state, excepting for the isotope ^{188}Pt. The SSA offers a very good description of the β band of these isotopes, especially for the isotopes ^{182}Pt and ^{186}Pt, respectively. In the γ band, some intermediate experimental energies are missing. For example, for the isotope ^{180}Pt the intermediate experimental energies 6^+ and 8^+ are not available, while for ^{188}Pt energies for 5^+ and 7^+ are missing. Concerning the γ band description, we can say that it is only partially well described and that because some states are well reproduced, while other not. This is not the case for the isotopes $^{190-196}$Pt where the DMA and SMA, besides the fact that are in good agreement with the experimental data corresponding to the ground and β bands, reproduce also the behavior of the γ band. For the isotope ^{196}Pt the experimental energy of 7^+ is missing.

In order to see which approach describes better the energy spectrum for all three bands of each isotope we give in Table 4 the root mean square (r.m.s.) values:

$$r.m.s. = \sqrt{\frac{\sum_{i=1}^{n}(E_{th.}^{(i)} - E_{exp.}^{(i)})^2}{n}}, \tag{24}$$

where, with n is denoted the number of states, while $E_{th.}^{(i)}$ and $E_{exp.}^{(i)}$ represent the theoretical and experimental energies of the ground, β and γ bands.

Table 4

The r.m.s. values for the energy spectra corresponding to the DSA, SSA, DMA and SMA given for the isotopes $^{180-196}$Pt.

Nucl	^{180}Pt		^{182}Pt		^{184}Pt		^{186}Pt		^{188}Pt		^{190}Pt		^{192}Pt		^{194}Pt		^{196}Pt	
	DSA	SSA	DSA	SSA	DSA	SSA	DSA	SSA	DSA	SSA	DMA	SMA	DMA	SMA	DMA	SMA	DMA	SMA
r.m.s. [keV]	83	58	72	47	104	83	106	107	31	45	40	71	52	76	36	69	47	92

Analyzing the r.m.s. values, we can see that the energy spectra of the isotopes ^{180,182,184}Pt are better described by the SSA than the DSA, for ^{186}Pt the r.m.s. values are closed to each other, while for the isotope ^{188}Pt the DSA is more appropriate. For the isotopes $^{190-196}$Pt, the balance is clearly inclined in the favor of the approach proposed here, namely, the Davidson and Mathieu Approach, comparing with the results of the SMA.

Some reduced B($E2$) transition probabilities are given in Tables 5,6 for each of the isotopes $^{180-196}$Pt.

Note that even the SSA describes better the energy spectra of the isotopes $^{180-184}$Pt than the DSA, for the transition probabilities the situation is reversed. For ^{186}Pt the DSA remains closer to the experimental data than the SSA. In the case of the isotopes ^{188}Pt and ^{190}Pt we can't compare the mentioned approaches due to the

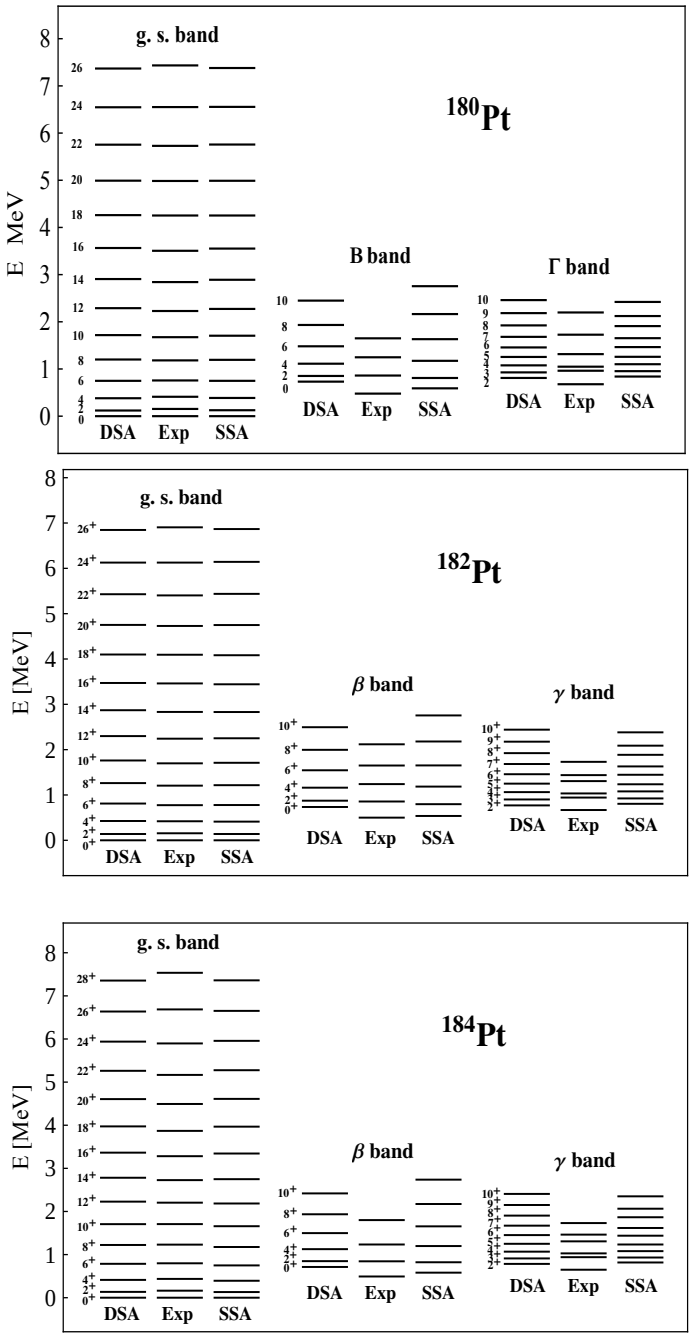

Fig. 2 – The energy spectra determined with the DSA and SSA are compared with the experimental data [36, 37, 39] of the isotopes ^{180,182,184}Pt.

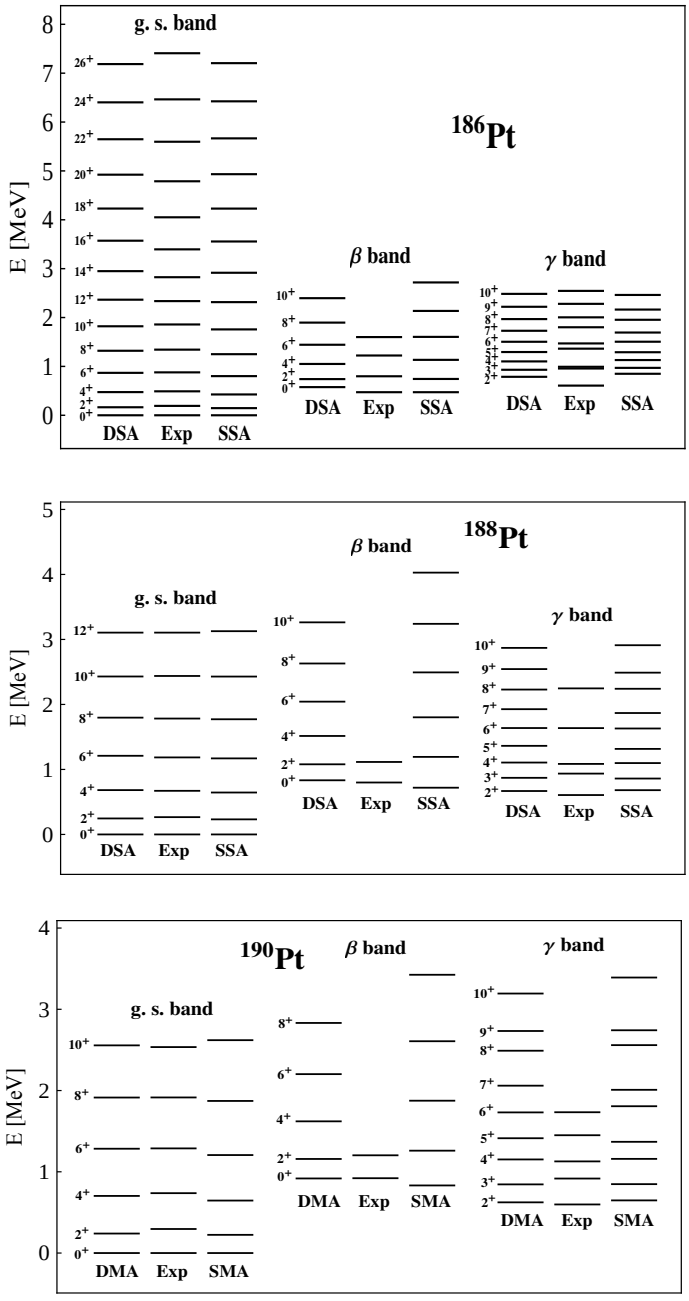

Fig. 3 – The energy spectra determined with the DSA and SSA are compared with the experimental data [38, 40] of the isotopes ^{186,188}Pt, while those of the DMA and SMA with the experimental data [41] of ^{190}Pt.

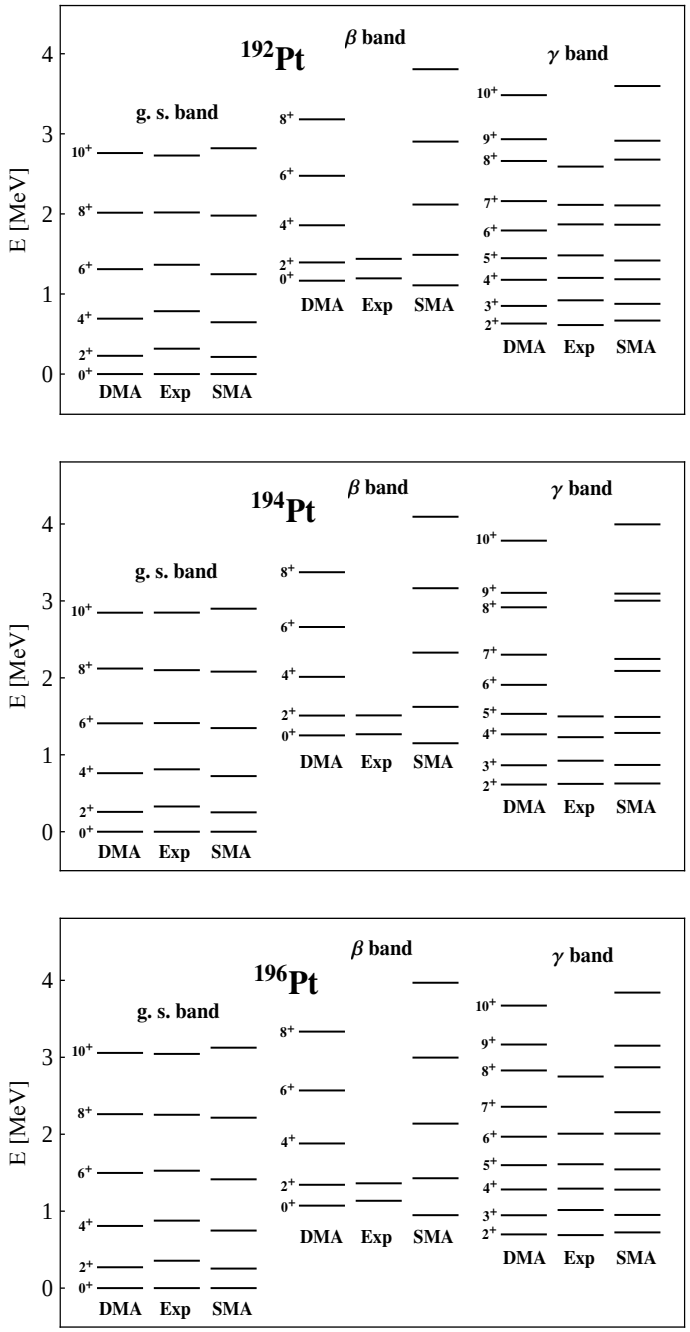

Fig. 4 – The energy spectra determined with the DMA and SMA are compared with the experimental data [42–44] of the isotopes ^{192,194,196}Pt.

lake of experimental data. Analyzing the results for $^{192-196}$Pt we can observe that the r.m.s. values of the SMA are a little better than those of the DMA.

As in the previous work [1], the contour plots of the squared wave function multiplied by the integration measure,

$$P(\beta,\gamma) = |f(\beta)\phi(\gamma)|^2\beta^4|\sin 3\gamma|, \tag{25}$$

are given in polar coordinates by using the transformation:

$$\int_0^\infty \int_0^{\frac{\pi}{3}} P(\beta,\gamma)d\beta d\gamma = \int_0^\infty \int_0^\infty P[\beta(x,y),\gamma(x,y)]\frac{dxdy}{\sqrt{x^2+y^2}}, \tag{26}$$

in order to see the shape of each isotope in the ground and some excited states. These plots are given in Figs. 5,6. These figures reflect the symmetry properties of the wave functions and Hamiltonian. Details about these properties were given in Ref. [1]. Note that if the results of the DMA from Fig. 6 are similar with those yielded by the SMA in Ref. [1], this is not the case if we compare the contour plots of the DSA with those of the SSA, especially for the isotopes ^{180,186,188}Pt for which the DSA predicts to have a triaxial deformation close to $\gamma_0 = 30^0$ rather than a shape close to an axial deformation. This difference between the DSA and SSA comes from the fact that in the γ equation of the SSA a term $-\frac{2}{3}\frac{1}{\langle\beta^2\rangle}L(L+1)$ is added from the β equation in order that the sextic oscillator equation for the β variable to be obtained. Therefore, this term leads to different values of the parameters u_1 and u_2 for the two approaches, and consequently to a difference in the behavior of the functions in the variable γ. Otherwise, the results of the DSA and SSA concerning the contour plots of the probability density would be similar.

Table 5

The B($E2$) transition probabilities yielded by the DSA, SSA, DMA and SMA are compared with the corresponding experimental data [8, 36, 38–41] of the isotopes $^{180-190}$Pt.

B($E2$) [W.u.]	^{180}Pt			^{182}Pt			^{184}Pt			^{186}Pt			^{188}Pt			^{190}Pt		
$J_i^+ \to J_f^+$	DSA	Exp	SSA	DSA	Exp	SSA	DSA	Exp	SSA	DSA	Exp	SSA	DSA	Exp	SSA	DMA	Exp	SMA
$2_g^+ \to 0_g^+$	110	153^{+15}_{-15}	110	163	108^{+7}_{-7}	167	165	127^{+5}_{-5}	176	153	113^{+8}_{-8}	162	82	82^{+15}_{-15}	82	56	56^{+3}_{-3}	56
$4_g^+ \to 2_g^+$	168	140^{+30}_{-30}	168	228	188^{+11}_{-11}	226	232	210^{+8}_{-8}	238	227	188^{+13}_{-13}	232	143		136	100		92
$6_g^+ \to 4_g^+$	206	≥ 50	202	239	284^{+18}_{-18}	232	248	226^{+12}_{-12}	243	259	289^{+23}_{-23}	254	202		171	143		116
$8_g^+ \to 6_g^+$	244		230	231	253^{+20}_{-20}	221	244	271^{+18}_{-18}	232	273	294^{+29}_{-29}	260	265		200	188		135
$10_g^+ \to 8_g^+$	285		255	210	266^{+21}_{-21}	204	227	310^{+10}_{-10}	214	272	304^{+26}_{-26}	258	329		226	235		152
$12_g^+ \to 10_g^+$	327		278	181	158^{+18}_{-18}	185	203	183^{+17}_{-17}	193	259	255^{+26}_{-26}	252	395		249			
$14_g^+ \to 12_g^+$	371		300	149	113^{+11}_{-11}	164	173	165^{+17}_{-17}	171	239	225^{+21}_{-21}	243						
$16_g^+ \to 14_g^+$							141	143^{+17}_{-17}	150	214	201^{+36}_{-36}	232						
$18_g^+ \to 16_g^+$							110	80^{+5}_{-5}	129									
r.m.s. [W.u.]	36		36	42		47	36		43	27		36						

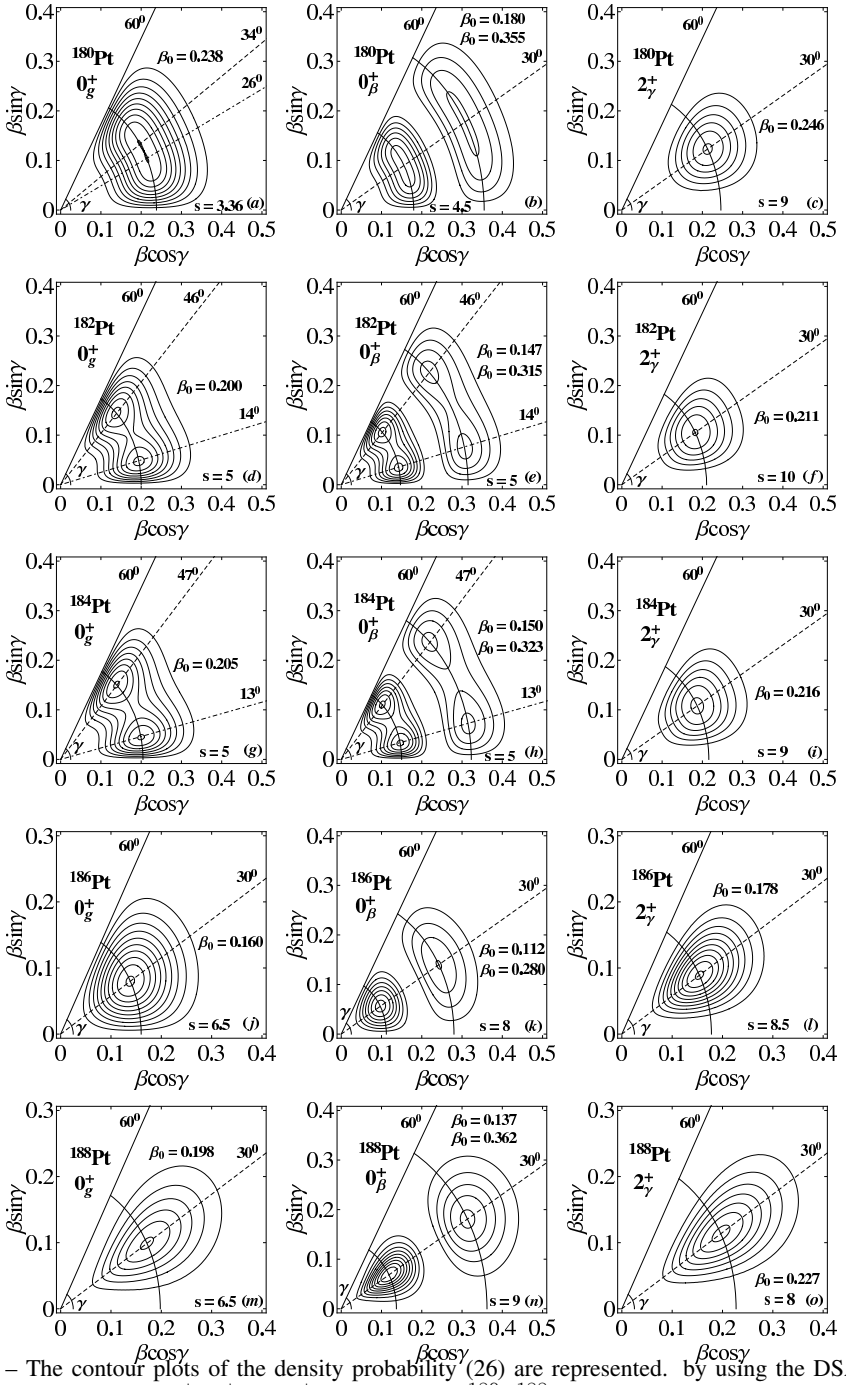

Fig. 5 – The contour plots of the density probability (26) are represented. by using the DSA wave functions, for the states 0^+_g, 0^+_β and 2^+_γ of the isotopes $^{180-188}$Pt. s is the step used in contour plots.

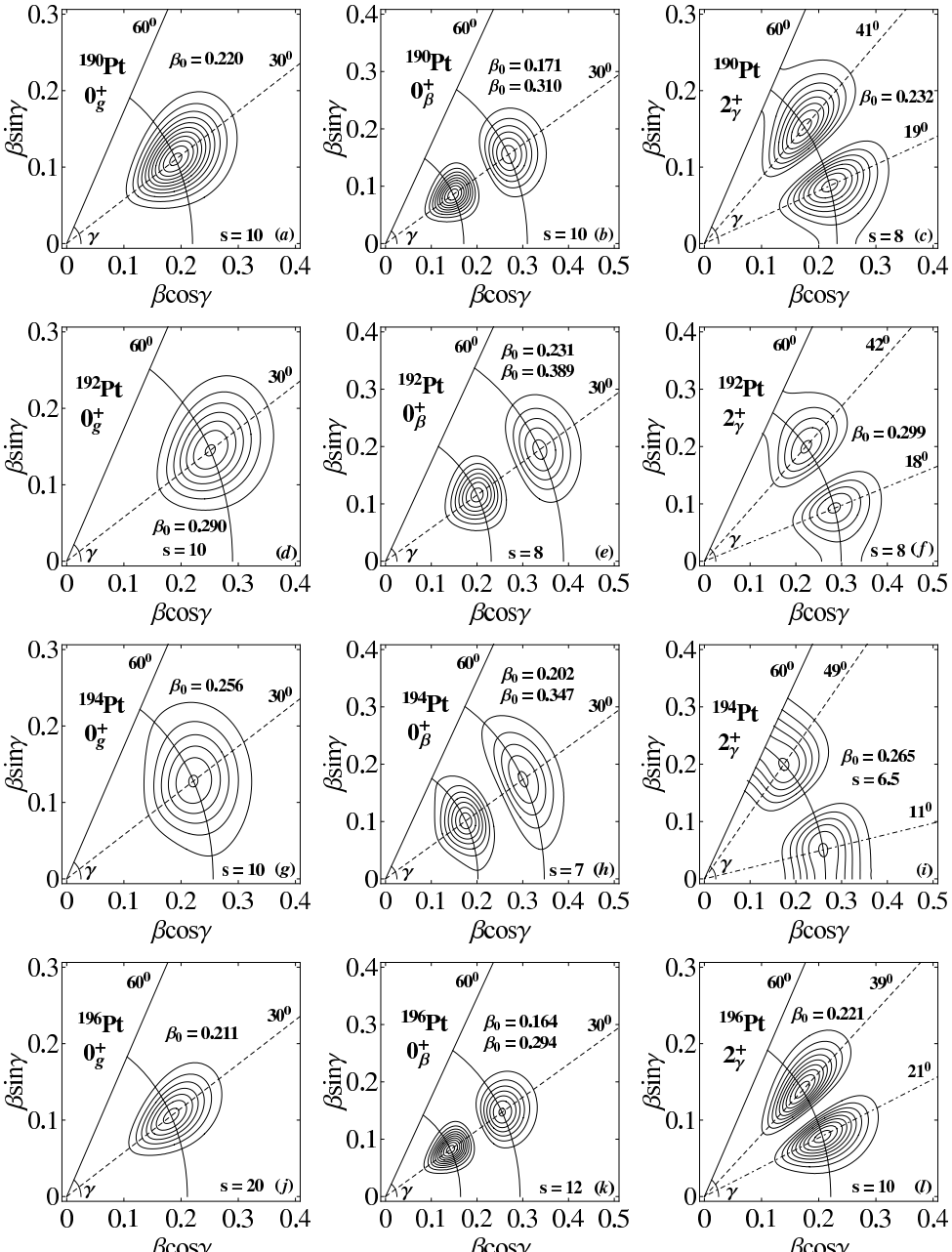

Fig. 6 – The contour plots of the density probability (26) are represented, by using the DMA wave functions, for the states 0^+_g, 0^+_β and 2^+_γ of the isotopes $^{190-196}$Pt. s is the step used in contour plots.

Table 6

The B($E2$) transition probabilities yielded by the DMA and SMA are compared with the corresponding experimental data [42–44] of the isotopes $^{192-196}$Pt.

B($E2$) [W.u.]	^{192}Pt			^{194}Pt			^{196}Pt		
$J_i^+ \to J_f^{'+}$	DMA	Exp	SMA	DMA	Exp	SMA	DMA	Exp	SMA
$2_g^+ \to 0_g^+$	48.7	$57.2^{+1.2}_{-1.2}$	49	22.4	$49.2^{+0.8}_{-0.8}$	24.9	30.4	$40.6^{+0.2}_{-0.2}$	34.1
$4_g^+ \to 2_g^+$	72	89^{+5}_{-5}	73	33	85^{+5}_{-5}	37	46	$60^{+0.9}_{-0.9}$	52
$6_g^+ \to 4_g^+$	100	70^{+30}_{-30}	98	47	67^{+21}_{-21}	51	66	73^{+4}_{-73}	72
$8_g^+ \to 6_g^+$				59	50^{+14}_{-14}	61	86	78^{+10}_{-78}	87
$10_g^+ \to 8_g^+$				72	34^{+9}_{-9}	70			
$2_\beta^+ \to 0_\beta^+$							37	5^{+5}_{-5}	23
$3_\gamma^+ \to 2_\gamma^+$	87	102^{+10}_{-10}	89						
$4_\gamma^+ \to 2_\gamma^+$				13	21^{+4}_{-4}	15	19	29^{+6}_{-29}	21
$6_\gamma^+ \to 4_\gamma^+$							27	49^{+13}_{-13}	29
$0_\beta^+ \to 2_g^+$				8.13	$0.63^{+0.14}_{-0.14}$	9.13	14	$2.8^{+1.5}_{-1.5}$	15.5
$2_\beta^+ \to 0_g^+$							0.2414	$0.0025^{+0.0024}_{-0.0024}$	0.1976
$2_\beta^+ \to 4_g^+$							13.07	$0.13^{+0.12}_{-0.12}$	9.83
$0_\beta^+ \to 2_\gamma^+$				0.4	$8.4^{+1.9}_{-1.9}$	0.5	0.2	18^{+10}_{-10}	0.2
$2_\beta^+ \to 2_\gamma^+$							7.87	$0.26^{+0.23}_{-0.23}$	7.81
$2_\gamma^+ \to 0_g^+$	1.00	$0.55^{+0.04}_{-0.04}$	0.93	0.97	$0.29^{+0.04}_{-0.04}$	1.29			
$2_\gamma^+ \to 2_g^+$				88	89^{+11}_{-11}	88			
$3_\gamma^+ \to 2_g^+$	1.86	$0.68^{+0.07}_{-0.07}$	1.74						
$3_\gamma^+ \to 4_g^+$	38	38^{+10}_{-10}	38						
$4_\gamma^+ \to 2_g^+$				0.60	$0.36^{+0.07}_{-0.07}$	0.79	0.25	$0.56^{+0.12}_{-0.17}$	0.32
$4_\gamma^+ \to 4_g^+$				20	14	19			
$6_\gamma^+ \to 4_g^+$							0.15	$0.48^{+0.14}_{0.14}$	0.19
$6_\gamma^+ \to 6_g^+$							10	16^{+5}_{-5}	10
r.m.s. [W.u.]	15		14	22		20	13		10

4. CONCLUSIONS

In the present work, a new solvable model for the quadrupole intrinsic variables was proposed, conventionally called the Davidson and Mathieu Approach (DMA). For the β variable a Davidson potential is used having as solutions the generalized Laguerre polynomials, while for the γ the Mathieu functions are the eigenstates by considering a periodic potential which may have a minimum around $\gamma_0 = 30$. The DMA together with its analogous, but for axial symmetric nuclei, the Davidson and Spheroidal Approach (DSA) were applied for the description of the ground, β and γ bands properties of the even-even isotopes $^{180-196}$Pt obtaining a good agreement with the corresponding experimental data. In a previous paper [1], this isotope chain was analyzed in the framework of other quadrupole solvable models, namely X(5), ISWSA, SSA, Z(5), ISWMA and SMA, respectively, with the best agreement with the experimental data in the favor of the SSA and SMA. In consequence, a comparison of the DSA and DMA numerical results with those of the SSA and SMA was

an interesting application in order to see what are the new contributions in explaining the experimental data brought by the present work. Therefore, the DSA offers a better description than the SSA for the energy spectra of ^{186,188}Pt and for the B(E2) transition probabilities of ^{180,182,184,186}Pt, respectively, while the DMA is clearly closer to the experimental spectra of the isotopes ^{190,192,194,196}Pt comparing with the SMA results. Concerning the axial shape deformations, the DMA results are similar with those of the SMA, while the DSA predicts a triaxiality close to $\gamma_0 = 30^0$ for the isotopes ^{180,186,188}Pt instead of axially deformed shape as predicted by SSA.

Acknowledgements. The authors acknowledge the financial support received from the Romanian Ministry of Education and Research, through the Project PN 09 37 01 02/2013.

REFERENCES

1. A. A. Raduta and P. Buganu, Phys. Rev. C **88**, 064328 (2013).
2. A. A. Raduta and P. Buganu, J. Phys. G: Nucl. Part. Phys. **40**, 025108 (2013).
3. A. A. Raduta and P. Buganu, Phys. Rev. C **83**, 034313 (2011).
4. A. Gheorghe, A. A. Raduta and A. Faessler, Phys. Lett. B **648**, 171 (2007).
5. F. Iachello, Phys. Rev. Lett. **87**, 052502 (2001).
6. D. Bonatsos, D. Lenis, D. Petrellis, P.A. TerzievPhys. Lett. B **588**, 172 (2004).
7. U. Garg *et al.*, Phys. Lett. B **180**, 319-323 (1986).
8. J.C. Walpe *et al.*, Phys. Rev. C **85**, 057302 (2012).
9. Liu Yuan *et al.*, Chinese Phys. Lett. **25**, 1633 (2008).
10. G. Dracoulis *et al.*, J. Phys. G: Nucl. Phys. **12**, L97 (1986).
11. G. D. Dracoulis, Phys. Rev. C **49**, 3324 (1994).
12. K. Nomura *et al.*, Phys. Rev. C **83**, 014309 (2011).
13. L. M. Robledo, R. Rodriguez-Guzman and P. Sarriguren, J. Phys. G: Nucl. Part. Phys. **36**, 115104 (2009).
14. P. Petkov, *et al.*, J. Phys.: Conf. Ser. **366**, 012036 (2012).
15. Kris Heyde and John L. Wood, Rev. Mod. Phys. **83**, 1467 (2011).
16. Irving O. Morales, Alejandro Frank, Carlos E. Vargas, P. Van Isacker, Phys. Rev. C **78**, 024303 (2008).
17. J. E. García-Ramos and K. Heyde, Nucl. Phys. A **825**, 39 (2009).
18. J. E. García-Ramos, K. Heyde, L. M. Robledo and Rodríguez-Guzmán, Phys. Rev. C **89**, 034313 (2014).
19. J. E. García-Ramos, V. Hellemans and K. Heyde, Phys. Rev. C **84**, 014331 (2011).
20. A. A. Raduta, A. C. Gheorghe, P. Buganu and A. Faessler, Nucl. Phys. A **819**, 46-78 (2009).
21. A. A. Raduta and P. Buganu, J. Phys.: Conf. Ser. **413**, 012029 (2013).
22. P. Buganu and A. A. Raduta, Rom. Journ. Phys. **57**, 1103-1112 (2012).
23. P. Buganu, A. A. Raduta and A. Faessler, J. Phys. G: Nucl. Part. Phys. **39**, 025103 (2012).
24. A. Bohr, Mat. Fys. Medd. Dan. Vid. Selsk. **26**, no.14 (1952); A. Bohr and B. Mottelson, Mat. Fys. Medd. Dan. Vid. Selsk. **27**, no. 16 (1953).
25. P. Van Isacker and K. Heyde, arXiv:nucl-th/1401.7512v1 (29 Jan. 2014).
26. L. Wilets and M. Jean, Phys. Rev.**102**, 788 (1956).

27. L. Fortunato, Eur. J. Phys. A **26**, s01, 1-30 (2005).
28. P. M. Davidson, Proc. R. Soc. **135**, 459 (1932).
29. Dennis Bonatsos, D. Lenis, N. Minkov, D. Petrellis, P. P. Raychev, P. A. Terziev, Phys. Lett. B **584**, 40 (2004).
30. J. P. Elliot, J. A. Evans, P. Park, Phys. Lett. **169**, 309 (1986).
31. D. Bonatsos, D. Lenis, E. A. McCutchan, D. Petrellis, I. Yigitoglu, Phys. Lett. B **649**, 394 (2007).
32. I. Yigitoglu and Dennis Bonatsos, Phys. Rev. C **83**, 014303 (2011).
33. Dennis Bonatsos, E. A. McCutchan, N. Minkov, R. F. Casten, P. Yotov, D. Lenis, D. Petrellis and I. Yigitoglu, Phys. Rev. C **76**, 064312 (2007).
34. Dennis Bonatsos, P. E. Georgoudis, D. Lenis, N. Minkov and C. Quesne, Phys. Rev. C **83**, 044321 (2011).
35. M. E. Rose, Elementary Theory of Angular Momentum (Wiley, New York, 1957).
36. S.-C. Wu and H. Niu, Nuclear Data Sheets **100**, 483 (2003).
37. Balraj Singh and Joel C. Roedinger, Nuclear Data Sheets **111**, 2081 (2010).
38. Coral M. Baglin, Nuclear Data Sheets **99**, 1 (2003).
39. Coral M. Baglin, Nuclear Data Sheets **111**, 275 (2010).
40. Balraj Singh, Nuclear Data Sheets **95** , 387 (2002).
41. Balraj Singh, Nuclear Data Sheets **99**, 275 (2003).
42. Coral M. Baglin, Nuclear Data Sheets **113**, 1871 (2012).
43. Balraj Singh, Nuclear Data Sheets **107**, 1531 (2006).
44. Huang Xiaolong, Nuclear Data Sheets **108**, 1093 (2007).